Finite element based modelling of the structural response of welded materials in complex loading configurations. Part I: Structural modelling considerations

A.J. Awang Draup[a,*], B. Rodgers[a], J.D Robson[a], P.B. Prangnell[a], Q.M. Li[a], M.J. Lunt[b]

[a]*The University of Manchester, Manchester, M13 9PL, UK*
[b]*DSTL, Porton, SP4 0JQ, UK*

Abstract

This two-part article presents the results of numerical prediction and experimental studies which aim to determine the structural response of friction stir welded aluminium 2139-T8 subjected to complex loading configurations, and in particular, air blast loading. The aim of this work is to develop a numerical modelling methodology to allow detailed prediction of the local strain evolution across the weld zone as this has significant influence in relation to structural response and failure. In particular, the method allows local material property gradients, which are due to variation in strengthening mechanism arising from microstructural damage caused by thermal loading during the welding process, to be incorporated into a macro scale structural model. Part I details the methodology used to implement local material property gradients together with experimental evidence to verify the predicted structural response in a range of loading configurations. Part II provides an insight into the assumptions made in Part I with respect to high strain rate materials modelling across the weld zone and the associated evidence for the variation in strengthening mechanisms in the alloy. The work presented highlights the importance of accurate description of the variation in local material properties, particularly the work hardening rate, in determining the response of structures under blast loading.

Keywords: Blast loading, Digital image correlation, Materials modelling, Finite element simulation, Materials characterisation

1. Introduction

The structural performance of welded structures subjected to air blast loading is of key interest to engineers and scientists across a range of industries. For civilian applications, typically the risk of air blast is due to gas explosions and is an important design consideration in the construction of offshore oil platforms [? ? ?]. A key consideration here is not necessarily just the initial damage from the blast loading, but the risk of subsequent injury from collapse of the remaining structure. For steel framed buildings that are common in civil engineering, plastic deformation in the joints, which may be manufactured by welding, can be the limiting factor controlling structural integrity [?]. Detailed understanding of this localised damage is extremely important when considering the potential resistance of a building to blast and, therefore, any required mitigating engineering works to reinforce the structure; this may have an impact on the cost or design layout of a structure.

For military applications, the use of welded joints is common in personnel transport vehicles. With an increase in the threat from Improvised Explosive Devices (IEDs), the performance of welded structures has come under scrutiny [?]. There has been a global trend towards the use of vehicles, such as the Mastiff, which are designed to be mine resistant [?]. In critical areas of a typical vehicle, such as the underbelly, the use of monolithic structures has become favourable as welds may lose integrity under blast loading. Local failure in the weld can lead to ingress of the explosive shock front into the vehicle, which can have catastrophic consequences on the occupants of the vehicle [?]. Indeed, it is unsurprising that one area of current research focus is on predictive techniques to aid the understanding of deformation and failure mechanisms in welded structures subjected to blast loading [? ? ?].

Of course, in order to model the non-linear behaviour of a welded structure accurately, it is necessary to understand the interrelation between materials processing, material microstructure and the subsequent material and mechanical properties. Furthermore, the application of numerical modelling techniques, alongside the intrinsic errors arising due to the modelling assumptions made, need to be fully understood if a high fidelity model of weld behaviour is to be utilised and interpreted correctly. The scope of this paper limits discussion to structures manufactured via Friction Stir Welding (FSW), as described in §??. Furthermore, discussion will be limited to heat treatable aluminium alloys, with particular reference to the alloy 2139-T8 as described in §??, though the general concepts are applicable across other alloys. Finally, consideration is only given to the Finite Element Method (FEM), as described in §1.1, since it is widely used as a tool to study the response of structures under a wide range of loading conditions.

1.1. Weld Modelling

The typical method to study structural response to loading is to use the FEM and there are many instances of its use to study

---

*Corresponding author. Tel: +44 (0)161 306 3578 Ext. 2261
Email address: `jefri.draup@manchester.ac.uk` (A.J. Awang Draup)

the response of welded structures [? ? ? ?]. However, successful macro scale modelling of weld behaviour under general loading conditions is extremely challenging as there are many factors which contribute to the overall structural behaviour. In addition to the variation in strengthening mechanisms across the weld zone (§??), phenomena such as geometry misalignment from the welding process, the formation of weld defects, and residual stresses are all complexities which contribute to structural performance [? ?]. For example, residual stresses are known to adversely affect the fatigue life of welded structures. Moreover, correct application of modelling technique, such as definition of loading and boundary conditions is pertinent to model quality. Whilst there has been a lot of work to improve FE based modelling methods with respect to some of the afore mentioned phenomena [? ? ? ?], a systematic approach to implementing local material property variation which arise due to welding process, which provides close quantitative correlation between prediction, has not emerged in the public domain.

In FEM based modelling, meso-scale complexity is typically dealt with by partitioning the mesh into distinct regions, which are representative of the weld regions (i.e. Nugget, TMAZ, HAZ and parent material) [? ?]. Elements are assigned to these partitions and are collectively assigned homogeneous isotropic properties; these are usually defined by a Johnson-Cook material model:

$$\sigma = \left(A + B\epsilon_p^n\right)\left(1 + C\ln\left(\frac{\dot{\epsilon}_p}{\dot{\epsilon}_{p0}}\right)\right)\left(1 - \left(\frac{T - T_0}{T_m - T_0}\right)^m\right) \quad (1)$$

It is common to assume that all parameters in equation 1 are the same as the parent material except for the A parameter; this is assumed to scale linearly with hardness. The geometry of each region, such as the HAZ, may be defined by examination of the hardness distribution in the cross section of an actual weld or by visual inspection of metallographic specimens. However, it is common practice to calibrate the geometry of the model to experimental data from a real weld loaded in uniaxial tension. Usually, the calibrated model is extended to more complex structures and loading configurations without any further modifications [? ?]. This approach will hereby be referred to as the "lumped-mass" method.

It is widely known that in reality, there can be local variation to thermal and strain rate sensitivity or work hardening rate across the weld region [? ?]. Since most weld models only account for yield stress variation across the weld important variation in material properties are neglected. As a result, strong material property gradients, which can be diffuse in nature, are over simplified when implementing step functions through the use of the lumped-mass method [? ?]. Further, important material property gradients across the weld, in particular the work hardening rate are ignored. These simplifications make it difficult to obtain good matching between the predicted non-linear structural response and experimental data, local to the weld zone. Careful calibration of the partitioned zones is required in order to match the global non-linear response of the weld [? ?]. Moreover, it is unclear whether a model calibrated to a particular loading condition, specifically uniaxial

tension, will accurately describe the structural behaviour under more complex loading conditions, such as blast loading of a plate. Data in the public domain reveal that structural models using the lumped-mass method only appear to show good qualitative correlation of structural behaviour of complex models calibrated to a more fundamental loading configuration; any supporting quantitative correlation is not reported [? ?].

1.2. Summary

In this paper, an attempt to implement the strong material property gradients arising due to changes in strengthening mechanism, which is linked to variation in local material microstructure, is made. In Part I, focus is made on implementing local property gradients and the application of this technique to simulate the behaviour of FSW 2139-T8 under complex loading configurations including explosive air blast. Furthermore, experimental evidence that supports the predictions made is also presented here. With respect to developing the specific material models, namely the Johnson-Cook model, these are detailed specifically in Part II.

2. Finite element modelling

Numerical modelling and simulation of welded panels was carried out using the commercial software package LS-DYNA version 971. In this study, the structural performance of welded material in two loading configurations was examined; tensile specimens loaded in uniaxial (cross weld) tension, and welded panels subject to blast loading. In all models, the dynamic response of the structure was analysed using explicit time integration methodology. A displacement-based (Lagrangian) finite element analysis based on the virtual work principle was used to model the equations of motion. By integrating the equations of motion through time, the conditions within a discretised model of the system were determined. In particular, the non-linear evolution of plastic strain across the weld region was of interest as it is linked to failure [?].

2.1. Model Geometry

In this study, 1:1 scale models of the experimental apparatus were built manually using HyperMesh (Figure 1). For all simulations, the welded structures were assumed not to contain any weld defects, such as porosity, kissing bonds, or root defects. Furthermore, it was assumed that there was neither misalignment of geometry arising from the welding process, nor any local weld flash. These assumptions were appropriate as care was taken to ensure samples were properly aligned during the welding process and the samples were machined to final geometry before testing. In all cases, 8-node solid hexahedron elements were used. In the weld region, the element mesh had a resolution equivalent to 1x1x1 mm. For the simulation of structures under blast loading (§??), the welded panels were bolted to a steel rig. These structures were meshed manually and were modelled using regular 8-node solid hexahedron elements; element distortion was minimised where possible in order to avoid volumetric locking during simulation. For the

washers, 4-node shell elements were used. Contact surfaces pairs were defined using the *CONTACT function between elements in direct contact with each other, such as the bolt, washer, locking nut, welded plate, and the supporting rig. For both the normal and tangential contact forces, these are defined by assuming frictionless contact force.

Figure 1: Example finite element mesh that was generated using the method in §2. Each colour code is indexed to a unique Johnson-Cook material modelled interpolated for the centroid of that element. The figure also highlights the node sets with boundary conditions specified in §2.4

2.2. Material Properties

For all modelled parts, Johnson-Cook material models were used to define plastic behaviour accounting for strain rate and thermal sensitivity. In the region of the weld (where the local mesh resolution is 1x1x1mm) each element in the weld cross section is assigned a unique Johnson-Cook material model. This allows strong gradients of material properties to be defined across the weld. For each unique material model, the parameters for equation 1 are defined based on the local thermal history, the post-weld hardness of the weld to be modelled, and mechanical property measurements obtained from "simulated weld material", as indicated by equations 2-6. By taking hardness measurements from three through thickness locations across the cross section of the weld in §3.1.1, a map of hardness at the centroids of each element in the mesh can be interpolated from theses measurements, and used to define the meso-scale geometry of the weld since hardness is an indicator of $f_i(T, t, \vec{x})$ in the weld. Simulated weld material is generated by heat treating parent material using equivalent thermal cycles for positions locally across the weld using a methodology described by Shercliffe [? ?]; this method can also be used to predict the post-weld hardness of a weld [? ?], which would allow prediction of weld structural response accounting for the welding parameters. Material property definition and, thus, meso-scale weld geometry is calibrated to a normalised weld condition rather than a particular loading configuration using this method, as is the case using the lumped-mass method. The Johnson-Cook parameters are shown to vary across the weld and are linked to changes in strengthening mechanism in response to the welding process. Further details of this method and experimental evidence for the link to strengthening mechanism variation are outlined in Part II the companion paper. An example of the parameters used to define material models for the elements across the weld cross section at the mid thickness of the plate are illustrated in figure 2.

$$A = k * Hv \tag{2}$$

$$B = f_1(T, t, \vec{x}) \tag{3}$$

$$n = f_2(T, t, \vec{x}) \tag{4}$$

$$C = f_3(T, t, \vec{x}) \tag{5}$$

$$m = f_4(T, t, \vec{x}) \tag{6}$$

Where

$$k = f_5(T, t, \vec{x}) \tag{7}$$

and $\vec{x}$ is the position of the element centroid within the welded sample; details are provided in Part II.

2.3. Loading Considerations

For all simulations, the presence of welding induced residual stresses has been neglected as it is assumed that they are relieved either during specimen preparation, when samples are sectioned from the welded plate, or during the initial stages of loading [?]. Moreover, implementation of a representative residual stress profile in FSW 2139-T8 [?] in the modelled scenarios demonstrated negligible influence on the structural performance of the welds, though these have been omitted for brevity. Typically, residual stresses have influence over the propagation of cracks, and, hence, fatigue life of a structure rather than the deformation behaviour under loading [?].

2.3.1. Uniaxial Loading Simulations

Loading due to gravity was ignored as these are small in comparison to the applied load and therefore unlikely to significantly affect the structural performance of the welds. Loading on the specimens was not explicitly defined using an applied external force, rather it was defined via the use of boundary conditions as detailed in §2.4.

2.4. Boundary Conditions
2.4.1. Uniaxial Loading Simulation

In the models of welds loaded in uniaxial tension, the nodes at the ends of the specimen were assigned a prescribed motion boundary condition (*BOUNDARY_PRESCRIBED_MOTION input card). The boundary conditions are illustrated in figure 1, and for the node set NS10001, the velocity is set to $u = 0$ mm min^{-1}, whilst for the node set NS10005, the velocity is set to $u = 1$ mm min^{-1}. This is equal to the velocity of the moving cross head on the tensile rig.

2.4.2. Blast Loading Simulation

For the blast loading prediction, a model of the entire experimental blast rig (figure ??) was built and the welded plate was constrained by bolts which attach the plate flush to the clamping structure. This was achieved with the use of frictionless contact surface pairs (see §2.1). The purpose is to allow pressure relief to the plate through deformation of the bolts. Unlike a model of a plate with fixed edge boundary conditions, modelling the entire rig does not artificially enhance the stiffness at the mounting points

3. Experimental Methods

In order to test the validity of the modelling method (§2) under a range of loading configurations, the structural performance of welds in both uniaxial and blast loading was measured experimentally in two studies. The details of the experimental methods used in both studies are detailed here.
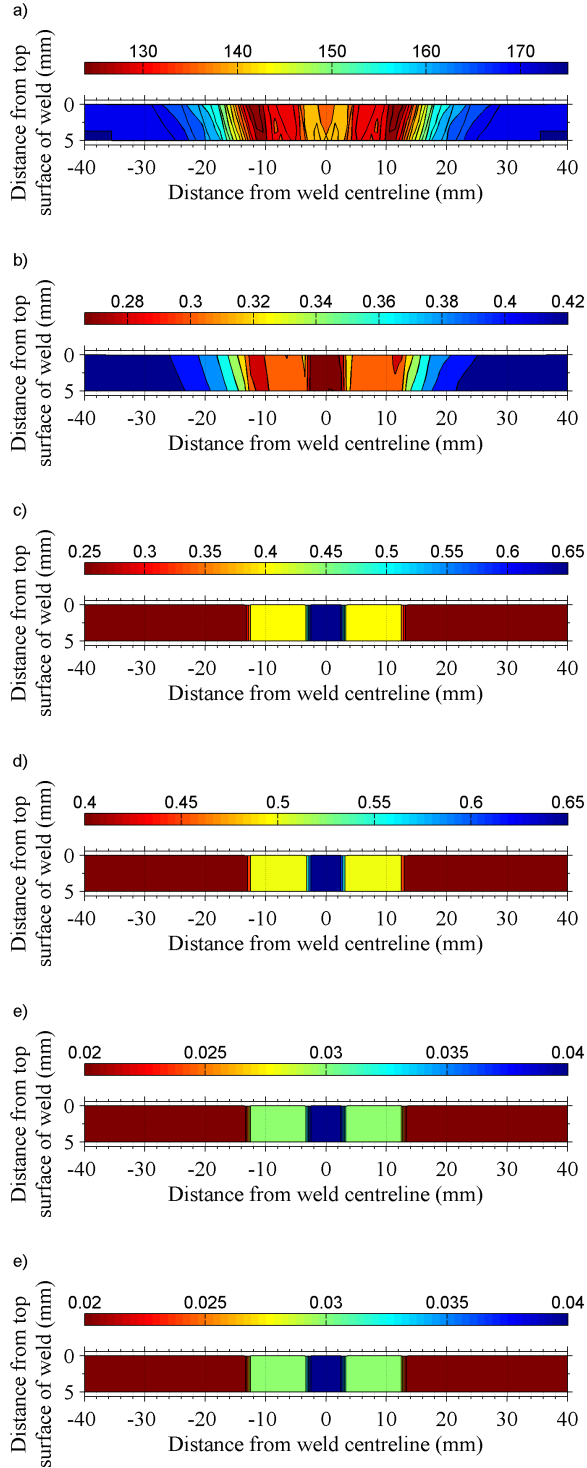
Figure 2: Element-wise distribution of properties interpolated across the weld cross section. a) Vickers Hardness b) Johnson-Cook A parameter (GPa). c) Johnson-Cook B parameter (GPa). d) Johnson-Cook n parameter. e) Johnson-Cook C parameter. f) Johnson-Cook m parameter.

3.1. Uniaxial Loading Configuration

This loading configuration was studied in order to verify the methodology of implementing local material properties in an FE model. Furthermore, the strain evolution in FSW 2139-T8 was measured experimentally to determine the accuracy of the modelling method.

3.1.1. Tensile Tesing of FSW 2139-T8

Bead on plate FSW was carried out on 2139-T8 alloy where the work-piece dimensions are 150x300x6.35 mm. Welding was carried out with a conventional tool with triflat pin set at a 2° rake angle. The tool dimensions were: 18 mm shoulder diameter; 2° shoulder concave angle; 6.2 mm pin root diameter; 5.85 mm pin height; 4 mm pin tip diameter. The weld settings were: 100 mm·min^{-1} traverse speed; 1000 RPM rotation speed; 16 kN downforce. The welds were carried out with the tool in force control mode. Square cross section bars with dimensions 5x5x150 mm were machined from the welded plates. By preparing samples in this way, geometry induced stress concentrations arising due to weld flash are eliminated as they are milled away. Further, residual stresses are relieved as the specimen is no longer constrained by the bulk material. This also simplifies the modelling process and allows the effects of material property gradients to be isolated during tests. Samples were tested using an Instron 5569 machine where the cross-head displacement rate was set to 2 mm·min^{-1}. Testing was carried out according to BS6892-1:2009.

3.1.2. Digital Image Correlation

2D Digital Image Correlation (DIC) was performed on square bar tensile specimens which captured the full weld region in order to measure the strain response of the weld. A LaVision Imager Pro Plus 4M greyscale camera, fitted with a Nikon AF-D Micro-Nikkor 105 mm f/2.8 macro lens and a Nikon 2x teleconverter, was used to acquire images with a 2096x2096 pixel resolution at a frequency of 1 Hz. The test setup was illuminated using a 150 W halogen lamp positioned at a low angle to the sample to avoid direct reflection into the camera. The specimens were prepared for DIC by first systematically grinding the face of the sample to be imaged down to 1600 grit. This ensures that the sample is flat, as required for 2D DIC, and has enough surface roughness to allow good adhesion between the paint and the sample surface. The surface was then thinly coated with a matt white surface primer; this prevents direct reflection of light into the camera. The sample was allowed to cure for 24 hours and was subsequently partially coated with a matt black spray paint. By partially coating the specimen, a unique speckle pattern forms naturally on the surface which can be analysed by the DIC software. The typical speckle feature size of the samples was approximately 3x3 pixels. DIC analysis was carried out using the commercial software package LaVision DaVis 8.1.5. A 2D time series cross correlation was carried out in integral mode using the sum of differential vector fields. Displacement calculation was performed with multi-pass iterations where the window sizes decrease from 128x128 pixels to 32x32 pixels. The final window had a circular Gaussian probability function

fitted to the sub-regions to account for large strains and rotations; all subregions were located with 25% overlap.

4. Results and Discussion

The relevant results and supporting discussion are split with reference to the particular loading condition studied. In particular, the focus of prediction and validation techniques pertains to the spatial and time evolution of plastic strain distribution across the weld. It is widely known that failure in ductile materials is often linked to the local plastic strain. In ductile materials, failure mechanisms such as formation of micro-voids, void coalescence and crack formation are heavily linked to plastic strain. Whilst there are many modelling methods which aim to predict these particular phenomena, they are not the focus of this study. The primary aim of the uniaxial tension study is to verify the prediction of strain distribution made using the modelling method in §2.3.1; the precise determination of failure is not considered. The primary aim of the blast loading study in §** is to verify that the modelling method in §** accurately captures the strain evolution when extended to complex loading configurations. Again the precise determination of failure is not considered.

4.1. Uniaxial Loading

The presented results can be understood upon examination of the material properties, which are linked to the strengthening mechanisms detailed in Part II. In this discussion, any variation in strengthening mechanisms shall be stated as all materials characterisation is discussed and justified in Part II. For the purposes of this discussion, the HAZ is split into the outer HAZ[1] and the inner HAZ[2]. The outer HAZ is the region between the hardness minima in the weld (see figure 2) and the parent material where the hardness value returns to that of the parent plate. The inner HAZ is the region bounded by the hardness minima in the weld and the dimensions of the tool pin. In this discussion the TMAZ is not treated as a distinct region in its own right, rather it is part of the inner HAZ. The nugget region is the region bounded by the dimensions of the tool pin[3].

On a macro scale, the evolution of strain is demonstrated in figure 3, which shows the distribution of the strain component in the cross weld direction; this is hereby referred to as axial strain. Most prominently, the features of interest which correlate closely between prediction and experimental evidence are the smooth gradients in strain in the outer regions of the weld; the correlation in strain throughout global deformation steps; and the single point of strain localisation in the weld. On a more local scale, figure 4 shows the distribution of axial strain at mid thickness of the weld cross section. The figure shows how strain evolves through time as strain is plotted at set global deformation steps (0.1 mm global displacement between the ends of the

[1]approximately the region of the weld cross section defined by $40 \geq |x| \geq 12$ mm

[2]approximately the region of the weld cross section defined by $12 \geq |x| \geq 3$ mm

[3]approximately the region of the weld cross section defined by $|x| \leq 3$ mm
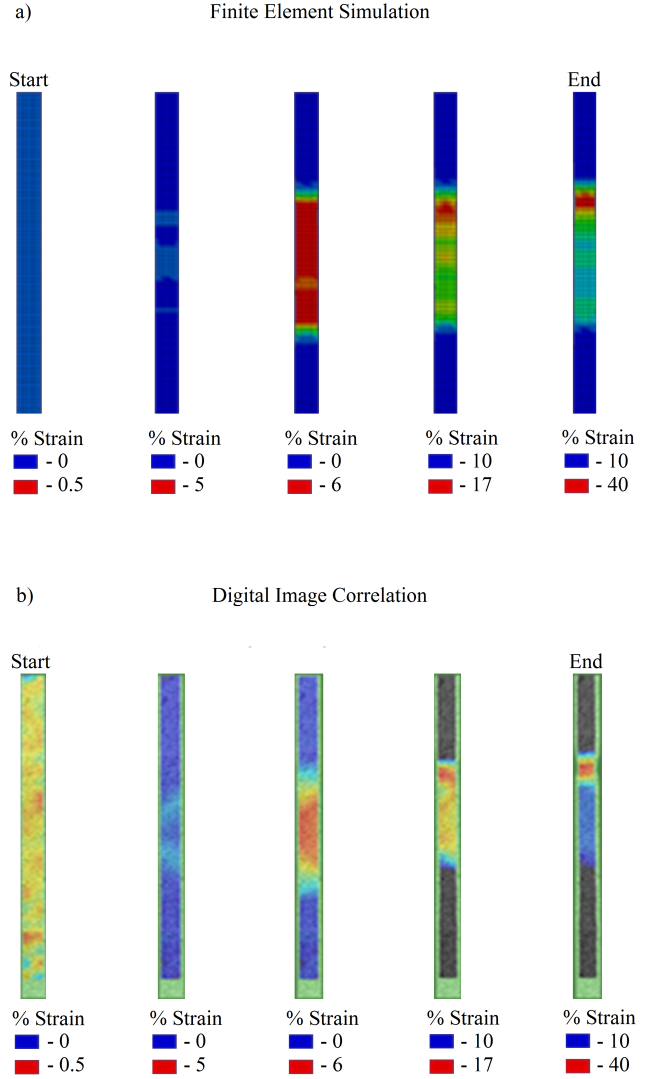

Figure 3: a) Predicted strain evolution using method in §2. b) Experimentally measured strain evolution using method in §3.1.2. In both figures, the cross-weld (x-direction) strain is plotted

sample). The evolution through time is illustrated by the transition of colour from blue, at the start of the test, to red, at the end of the test. The figure allows comparison of the predicted strain using the method in §2 and experimentally measured strain using the techniques in §3.1. The experimental evidence shows that during the early stages of deformation, axial strain appears to be distributed across the inner regions of the weld (nugget and TMAZ). Axial strain then increases, and is most prominent, in these innermost regions of the weld zone but also occurs in the HAZ. All of the axial strain does, however, appear to be confined to the weld zone, or the region defined by the width of the HAZ. Axial strain continues to increase until a critical point, with respect to global deformation of the sample, when it begins to localise (approximately -12 mm from the weld centreline) within the weld zone. The axial strain is distributed

uniformly within the inner regions of the weld and measures approximately 15%. As the strain localises in the weld zone, it rapidly increases to approximately 22% before failure. In line with experimental evidence, the prediction using the method in §2 shows that axial strain is distributed across the inner regions of the weld during the early stages of deformation, and is greatest in the nugget. Strain increases across the weld, as the sample is loaded, but remains confined within the weld zone. Axial strain continues to increase until a critical point, with respect to global deformation, when it begins to localise approximately -12 mm from the weld centreline. Axial strain varies between 10-15% across the inner regions of the weld but remains stable, whilst localisation causes a rapid increase in strain towards the end of the simulation. The predicted geometric distribution of strain through deformation appears to correlate closely with experimentally measured results. In addition, the position of strain localisation is predicted accurately.

Upon examination of the variation initial flow stress across the weld (see figure 2), it is clear that initial deformation will occur in the nugget region since this region has the lowest flow stress. This is in line with materials data on FSW 2139-T8 reported by Gruijicic [**?**], though data from McWilliams [**?**] shows that the TMAZ in 2139-T8 welds can exhibit the lowest initial flow stress. However, the reported weld conditions together with micrographs indicate that the thermal cycles in those welds were quite low [**?**]. It is possible that the overall variation in strengthening mechanisms in these studies are different to those described in Part II. Deformation behaviour of 2024 alloy, as reported by Genevois [**?**] and Sato [**? ? ?**], also shows initial yielding in the nugget region and the contributors to strengthening mechanisms are similar to the conclusions from Part II. Since there is no description of the strengthening mechanisms by McWilliams or Grujicic the cause of initial yielding in their studies is unclear. However, it is possible that the difference is linked to the markedly different welding parameters, and therefore the thermal loading, used in each study [**?**]. As the nugget region work hardens, the surrounding region (TMAZ and inner regions of the HAZ) begins to deform since the flow stress is equal to that of the nugget region. Since the nugget region has a greater work hardening rate than the immediate surrounding material [**? ?**], strain will not, in theory, localise here except in the presence of some defect. The high work hardening rate of nugget material as compared to material elsewhere in the weld or parent material in age hardened alloys has also been reported by Karlsson [**?**] and Mahoney [**?**] and is generally true for peak hardened aluminium alloys subjected to FSW. As strain develops it is mainly distributed across the inner regions of the weld zone until a critical point where it localises just outside the position of minimum hardness of the weld; the hardness minima represents the boundary between the inner and outer HAZ, as shown in Part II. However, this is not generally true and depends on the initial aging condition. Further, some 7xxx alloys, for example, have several kinds of second phase precipitate which contribute to strengthening [**?**]. Each precipitate may respond differently to the thermal cycle and it is not necessarily the case that the hardness minima and strengthening mechanism variation are correlated. Strain

begins to localise when the inner regions of the weld have work hardened to a point where the flow stress is equal to or greater than the minimum flow stress of the outer HAZ (the boundary of the inner and outer HAZ). Combined with the gradient in flow stress in the outer region of the HAZ, which forces strain localisation towards the centre of the weld, since the work hardening rate of the inner regions of the weld is much greater than the outer HAZ, strain should theoretically begin to localises just outside the hardness minima.

In 2139-T8 alloy, from the results presented in Part II, the changes in strain rate across the weld are linked to the variation in strengthening mechanism induced by the welding process. The parent material has low work hardening rate due to high dislocation density from processing and the dominance of the Ω strengthening phase. The outer HAZ has similar work hardening rate because, even though dislocation density is reduced (through dislocation annihilation processes arising from thermal loading) and Ω phase is coarser and less finely distributed than the parent phase having overaged from the T8 condition [**?**], the dominant strengthening mechanism is still the same as the parent material. In the inner regions of the HAZ, TMAZ, and nugget the temperatures are high enough to cause dissolution of Ω on a local scale and further annihilate dislocations; the precise location where this occurs coincides with the hardness minima in the weld cross section. Hence, in these inner regions, contribution from strengthening mechanisms such as solid solution strengthening and the formation of Guinier-Peston (GP) zones after natural aging become important [**? ? ?**]. Ω phase does not re-precipitate out because there is no controlled heat treatment process after the welding proces. Whilst grains in the TMAZ have undergone severe plastic deformation, they are still of the same order of magnitude as the parent material and outer HAZ. However, grains of the nugget have undergone dynamic recrystallisation due to the combination of thermal loading and plastic deformation. The effect of grain size refinement becomes an additional contributor to strengthening mechanism in this region [**? ?**]. Therefore, if we consider the distribution of material properties in figure 2, the distinct changes work hardening rate are physically reasonable. Indeed, the smooth gradient in flow stress up to the location of the hardness minima, and the uniform distribution of flow stress in the inner regions of the HAZ which only change within the nugget are also physically reasonable.

It is clear that the accurate description of material properties, which is linked to the variation in strengthening mechanism in the welded alloy, has facilitated the prediction of the evolution of strain distribution in the weld. Whilst no attempt is made to determine failure in the model, it is clear that using the §2 modelling approach, the precise location of strain localisation can be determined and the evolution of strain is within order of magnitude and close to experimentally measured evidence. Implementing a failure model linked to strain is likely to match using the presented modelling method.

4.2. Joint observations

Both the quantitative and qualitative data presented in §4.1 and §**??** indicate that the implementation of material property
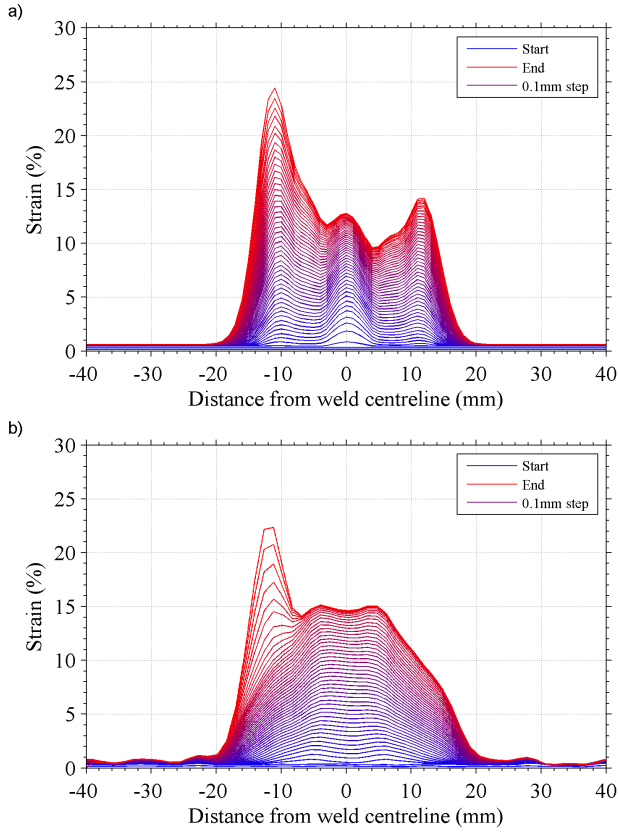
a)

b)

Figure 4: a) Predicted strain evolution using method in §2. b) Experimentally measured strain evolution using method in §3.1.2. In both figures, the cross-weld (*x*-direction) strain is plotted for the mid thickness of the welded plate. In addition, the colour transitions from blue at the start of the test to red at the end of the test; each plot line is for a global displacement between the ends of the sample of 0.1 mm.
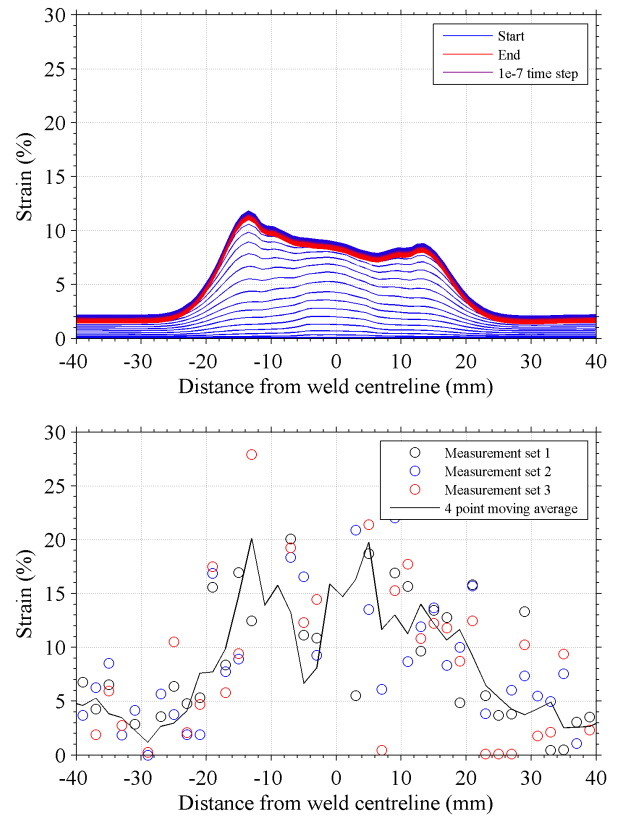

Figure 5: a) Predicted strain evolution using method in §2. The colour transitions from blue at the start of the test to red at the end of the test; each plot line is for a time step of 0.1ms. b) Experimentally measured surface strain using method in §**??**. In both figures, the cross-weld (*x*-direction) strain is plotted for the surface of the welded plate.

gradients induced by variation in strengthening mechanisms lead to accurate prediction of strain response in space and time dimensions. The method allows the prediction of complex structural behaviour, which varies depending on the loading conditions of a structure. The method described in §2 differs significantly from the typical methods described in the public domain. The methods in the public domain typically give good correlation in the predicted global strain response of a weld when calibrated to an experiment of a weld in uniaxial loading condition [**? ?**]. However, the typical approaches often lead to poor local correlation in strain response and erroneously predict the double strain localisation effect in uniaxial tension. When the methods are extended to more complex blast loading configurations, only qualitative correlation of strain response is reported in the public domain; this may be due to the fact that papers on this subject are proprietary in nature. However, given that the methods give erroneous prediction of strain response when calibrated to a particular loading configuration, it is unclear whether the qualitative correlation in complex configurations is coincidental [**? ?**].

5. Conclusions

In this study, an FE based modelling method, which incorporates element-wise material property variation to detail the strong material property gradients arising from the welding process, was utilised to predict the structural response of FSW 2139-T8 under complex loading configurations, including blast loading. The method requires an understanding of the strengthening mechanism variation in FSW 2139-T8 and is only feasible through automation of the mesh building process. The method utilised removes the need to calibrate models geometry to a particular loading configuration, rather it is calibrated to a normalised weld condition; this removes modelling errors which may arise when extending models to study structural performance under different loading configurations. Moreover, this allows the method to be used to study the effect of welding parameters on structural performance, potentially enabling numerical weld optimisation, which is theoretically applicable to any heat treatable aluminium alloy. The method has been verified experimentally using DIC for FSW 2139-T8 in under uniaxial tension. The method provides good correlation for strain evolution both globally and locally across the weld zone; this represents an improvement over existing techniques reported in the public domain. Furthermore, strong supporting experimen-
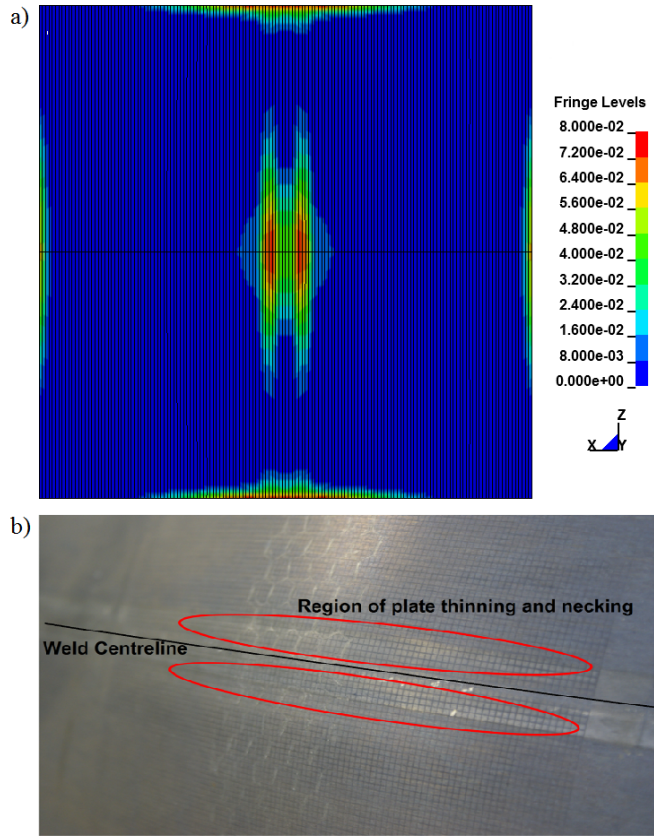
Figure 6: a) Example of the double strain localisation effect predicted under blast loading. b) Observed thinning in welded plates subjected to blast loading which occurs in two locations either side of the weld centreline.

tal evidence has been generated which indicates that the method provides good qualitative and quantitative correlation with experimental evidence when extended to more complex loading configurations; this represents an improvement on modelling techniques available in the public domain.

References